Small-angle neutron scattering by a xerogel of a solid solution of oxides of titanium, tin, and zirconium

É. Z. Valiev, S. G. Bogdanov, Yu. A. Dorofeev, A. N. Pirogov, L. M. Sharygin, V. I. Barybin, and O. Yu. Smyshlyaeva

Institute of Metal Physics, Ural Branch of the Academy of Sciences of the USSR

(Submitted 28 February 1991)
Zh. Eksp. Teor. Fiz. **100**, 1000–1008 (September 1991)

The intensity of the small-angle neutron scattering by xerogel samples annealed at various temperatures has been measured over the scattering-vector interval $q = 0.008$–0.5 Å^{-1}. The peak on the scattering curves is interpreted on the basis of the Porod model for a porous structure. The correlation lengths of the pore structure are determined. The asymptotic behavior as $q \to \infty$ of the scattering curves is q^{-n} with $n \sim 3.65$–4. This is the behavior typical of the fractal surface of a solid phase for $n < 4$. The correlation lengths and specific surface areas found for the porous structure from the small-angle scattering are compared with the values found for these properties by other methods.

INTRODUCTION

Small-angle neutron scattering is used widely to study highly dispersed porous materials and other structures which grow in random processes.[1,2] In particular, small-angle neutron scattering can be used to study the fractal characteristics of objects. For fractals, the scattering intensity is typically a power-law function of the momentum transfer $q = 4\pi\sin\theta/\lambda$, where λ is the neutron wavelength, and 2θ is the scattering angle:

$$I(q) \sim q^{-n}, \tag{1}$$

where n is the Porod exponent. The q interval in which (1) holds is the "Porod region" of the scattering curve.

For three-dimensional and bulk fractals, n is the same as the fractal dimensionality D, where $1 \leqslant D \leqslant 3$. For scattering by three-dimensional entities with fractal surfaces we would have $n = 6 - D_S$, where D_S is the fractal dimensionality of the surface ($2 \leqslant D \leqslant 3$). In addition, for fractal porous materials we would have $n = 7 - \gamma$, where γ is the exponent in the distribution of pores with respect to the size r:

$$P(r) \sim r^{-\gamma}. \tag{2}$$

Most of the studies on small-angle neutron scattering by porous objects have not, however, determined quantitative characteristics of the porous structure. Outside the Porod region, at small values of q, certain materials have a peak on their scattering curve which is believed to be unrelated to the porous structure of the sample.[3]

Our purpose in the present study was to obtain quantitative information about the porous structure of xerogels of solid solutions from experiments on small-angle neutron scattering. These materials, with their large surface area, are used as sorbents in catalysis, chemistry, and nuclear power. They also hold promise in electronics and other technological fields. We interpret the data on small-angle neutron scattering by these objects with the help of the model described in Ref. 4, of a randomly distributed substance of homogeneous density, as proposed by Porod.[5] That approach makes it possible to analyze the entire scattering curve, rather than simply the Porod region. We also compare the data from small-angle neutron scattering on the length scales and area scales of the internal surfaces with the corresponding values found from large-angle diffraction and from experiments on low-temperature adsorption of nitrogen vapor.

1. TEST SAMPLES AND EXPERIMENTAL PROCEDURE

A solid solution of the oxides, with the composition 40 mole % TiO_2, 55 mole % SnO_2, and 5 mole % ZrO_2, was prepared by the sol-gel method[6] in the form of spherical grains 1–3 mm in diameter, with a saturation density $\rho_{sat} \simeq 1.6$ g/cm^3. The test samples were annealed in vacuum for 1 h at 150–900 °C. A total of eleven samples, differing in annealing temperature, were studied (Table I). For all samples, x-ray diffraction patterns at large angles were recorded in order to determine the atomic structure and the size of the coherent-scattering regions. The characteristics of the porous structure were determined from data on nitrogen absorption and on small-angle neutron scattering. The small-angle neutron scattering was measured on two pieces of apparatus, installed in horizontal experiment channels at the IVV-2 reactor. The measurements in the interval $q = 0.008$–0.13 Å^{-1} were carried out on a small-angle neutron scattering device with an average neutron wavelength $\bar{\lambda} = 4.5$ Å with $\Delta\lambda/\lambda \simeq 30\%$. The measurements in the interval 0.09–0.5 Å^{-1} were carried out on an apparatus with a monochromatic neutron beam with $\lambda = 2.42$ Å. The scattered-neutron intensities were converted into scattering cross sections with the help of a standard vanadium sample. All the measurements were taken at room temperature.

2. EXPERIMENTAL RESULTS AND DISCUSSION

According to the results of the neutron diffraction and the large-angle x-ray diffraction, all the samples of the original composition were solid solutions with a tetragonal unit cell (of the rutile type), with lattice constants $a = 4.70$ Å and $c = 3.12$ Å and with six atoms. The x-ray density found for the solid phase from these data is 5.83 g/cm^3; the volume fraction of the solid phase in the porous sample is found to be $c \simeq 0.5$.

Figure 1 shows the angular distribution of the neutron

 0038-5646/91/090552-05$03.00

TABLE I. Characteristics of the porous structure of a xerogel of a (Sn, Ti, Zr) O_2 solid solution.

Sample	Annealing temperature, °C	S_{N_2}, m^2/g	d, Å	d_K, Å	L_c, Å	Porod exponent	S, m^2/g
1	150	243	42	46	—	4,00±0,15	192
2	200	208	50	44	—	4,00±0,15	169
3	250	185	56	48	20	—	—
4	300	166	62	56	—	3,95±0,15	118
5	350	130	80	—	26	—	—
6	400	110	94	—	42	3,72±0,15	103
7	500	90	114	72	56	3,7±0,15	85
8	600	76	136	—	69	3,65±0,10	72
9	700	67	154	86	70	—	—
10	800	42	244	108	98	3,65±0,10	52
11	900	24	428	288	—	3,65±0,10	25

scattering cross section for several samples. These curves have peaks at q between 0.02 and 0.05 $Å^{-1}$. There is no peak on the curve for the sample annealing at 900 °C; this peak presumably does exist, but at angles inaccessible in our experiments. The error in the determination of the scattering cross section is not indicated in this figure. This error might amount to several tenths and would come into play in the conversion of the measured intensities into cross section, because of the uncertainty regarding some of the nuclear-physics properties of the sample material.

It can be seen from Fig. 1 that with increasing annealing temperature the peak on the scattering curve shifts toward smaller angles, and the scattering cross section increases dramatically. It is natural to link these effects with enlargement of the solid-phase particles as they are sintered during the annealing. The same conclusion is implied by analysis of the experiments on the adsorption of nitrogen vapor and by the results found on the dimensions of the coherent-scattering regions from the width of the Bragg reflections. These dimensions were estimated under the assumption that the original grains had a globular structure consisting of microscopic spherical particles of diameter d_{coh}, a certain packing of which forms a porous structure.

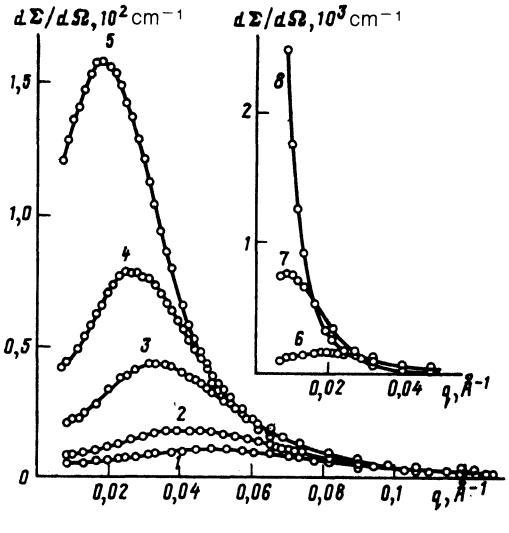

FIG. 1. Differential cross section for small-angle neutron scattering by a unit volume of (Sn, Ti, Zr)O_2 xerogel samples annealed at various temperatures. 1—250 °C, 2—350 °C, 3—400 °C; 4—500 °C; 5—600 °C; 6—700 °C; 7—800 °C; 8—900 °C.

In the experiments on the absorption of nitrogen vapor, we determined the specific inner surface area S_{N_2}; the average surface diameter of the particles (globules) was found from the expression

$$S_{N_2} = \frac{6}{d\rho_{sol}},$$

where ρ_{sol} is the actual density of the solid phase.

Table I shows the specific surface area S_{N_2}, the corresponding surface diameter d, and the size of the coherent-scattering regions, d_{coh}. The errors in the determination of these properties include the errors of the experimental procedures and also the imperfections of the model of the porous structure. They are apparently of the same magnitude as the error in the determination of the neutron scattering cross section. We see from this table that the characteristic structural dimensions determined for the samples by the different methods are approximately the same and can be used in analyzing the data on small-angle neutron scattering.

The asymptotic behavior as $q \to \infty$ of all the scattering curves in Fig. 1 is a power law $d\Sigma/d\Omega \sim q^{-n}$ with n between 3.65 and 4.0.

We will first discuss the small-angle neutron scattering curves near the peak and then move on to the behavior of the scattering cross section in the limit $q \to \infty$.

2.1. Model of the porous structure and its application in analyzing the small-q scattering cross section. In general, the model of a set of microscopic particles or a globular model of the porous structure can be used in interpreting scattering curves of a xerogel if one assumes that the microscopic particles interact as the molecules of a liquid or solid do. Results on the scattering by concentrated oxide sols were explained in this manner in Refs. 7 and 8. However, we use a different model here, which we feel is more appropriate for a xerogel. This is a model of a randomly distributed substance of homogeneous density.[4] This model is frequently used in analyzing the asymptotic behavior as $q \to \infty$ of the cross section for scattering by porous objects.

According to this model, the differential cross section for the scattering of neutrons by a unit volume of a porous solid is

$$\frac{d\Sigma}{d\Omega} = 4\pi\rho^2 c(1-c)\int_0^\infty \gamma(r)\frac{\sin qr}{qr} r^2\, dr, \qquad (3)$$

where c is the volume fraction of the solid phase, $\rho = \bar{b}n/v^3$ is the amplitude density of the neutron scattering, $\bar{b}$ is the average neutron scattering amplitude, v is the volume of the unit cell, n is the number of atoms in the unit cell, and $\gamma(r)$ is a correlation function, given by

$$\gamma(r) = \frac{Z(r)-c}{1-c}. \tag{4}$$

Here $Z(r)$ is the probability (averaged over all points of the sample and over all directions) that, if some point lies in the region occupied by the solid phase, then a second point, at a distance r from the first, also lies in the region occupied by the substance.

The limiting values of $\gamma(r)$ are known: $\gamma(r) \to 1$ as $r \to 0$ and $\gamma(r) \to 0$ as $r \to \infty$. It follows from the definition (4) that as r increases from 0 to ∞ the function $\gamma(r)$ can oscillate around a value of zero, changing sign when the point of the vector **r** goes out of the substance into a pore or vice versa. The amplitude and period of these oscillations should fall off monotonically with increasing r. In general, on the other hand, $\gamma(r)$ is a characteristic of a porous structure, which determines the short-range order in the distribution of the substance and the voids and also the characteristic dimensions of both.

The scattering at small angles determines the behavior of $\gamma(r)$ at large distances. Taking the oscillatory nature of $\gamma(r)$ into account, we adopt it in the form shown in the inset in Fig. 2. Substituting $\gamma(r)$ into (3), and using an approximation as used by Guinier,[4] we find an expression which holds for $qR \lesssim 1$:

$$\frac{d\Sigma}{d\Omega} = \frac{4\pi}{3}\rho^2 c(1-c)\left[(\gamma_1+\gamma_2)R_1^3 \exp\left\{-\frac{q^2R_1^2}{10}\right\} - \gamma_2 R_2^3 \exp\left\{-\frac{q^2R_2^2}{10}\right\}\right]. \tag{5}$$

The solid lines in Fig. 2 are calculated from (5) for various values of R_1. In these calculations we used the values $c \simeq 0.5, \rho^2 = 16.5 \cdot 10^{20}\,\text{cm}^{-4}, R_2/R_1 = 1.414, \gamma_2/(\gamma_1+\gamma_2) = 0.3$, and $\gamma_2 = 0.3$.

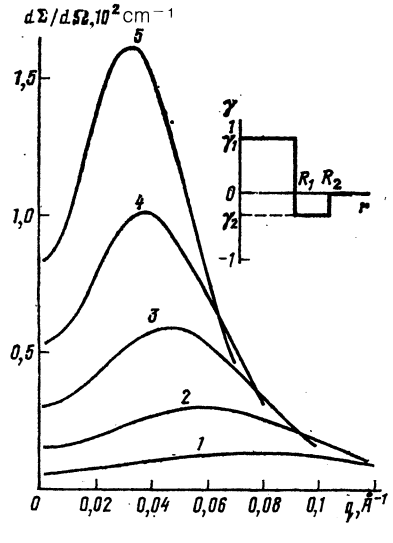

FIG. 2. Differential cross section for neutron scattering calculated from (5). The inset shows the function $\gamma(r)$ used in the calculations. The values of R_1 for curves 1–5 are 30, 40, 50, 60, and 70 Å, respectively.

It can be seen from a comparison of the curves in Figs. 1 and 2 that the theoretical curves agree satisfactorily with the experimental ones in terms of both the absolute value of the cross section and the shape. Admittedly, we would have to use a more realistic function $\gamma(r)$ in order to extract quantitative information, and we would have to determine the parameters of this function by fitting the experimental data or by using inverse Fourier transforms. Nevertheless, we believe that the oscillatory nature of $\gamma(r)$ has now been solidly established. We should not assume that the oscillatory function which we have adopted for $\gamma(r)$ is of universal applicability—that it is valid for all porous structures. For example, Debye *et al.*[9] found a function $\gamma(r) = \exp\{-r/a\}$ for a structure with a completely random shape and a completely random pore distribution. We might note the analogy between (on the one hand) the scattering curves of the porous structure and (on the other) the scattering by Guinier-Preston zones and by ordered alloys with a short-range order.[10] This analogy is not purely superficial; it rests on a similarity in the physical processed involved in the formation of these structures.

Let us find some global properties of our model. As was shown in Ref. 4, the correlation length is

$$L_c = 2\int_0^\infty \gamma(r)\,dr = [2\pi\rho^2 c(1-c)]^{-1}\int_0^\infty q\frac{d\Sigma}{d\Omega}\,dq. \tag{6}$$

Correlation lengths calculated from the experimental data with the help of Eq. (6) are given in Table I. We see that these lengths are close to the dimensions of the coherent-scattering regions.

It is interesting to compare the correlation length calculated with the function $\gamma(r)$ in Fig. 2 with the length L_c found experimentally. The curve for $R_1 = 50$ Å in Fig. 2 is approximately the same as the curve for a sample annealed at 500 °C in Fig. 1. The correlation length for a step function $\gamma(r)$ and for $R_1 = 50$ Å is 58 Å according to (6). For the sample annealed at 500 °C we have $L_c \simeq 56$ Å. In other words, even the step function $\gamma(r)$ in Fig. 2 is good for some quantitative estimates.

In our case, an integral Porod invariant should exist:[4,11]

$$Q = \int_0^\infty q^2\frac{d\Sigma}{d\Omega}\,dq = 2\pi^2\rho^2 c(1-c). \tag{7}$$

Since all the samples have the same chemical composition and the same volume fraction of solid phase, the quantity (7) has the same value for the various curves in Fig. 1. Substituting numerical values for ρ and c into (7), we find

$$Q = 2\pi^2\rho^2 c(1-c) = 8{,}15 \cdot 10^{21}\,\text{cm}^{-4}.$$

An evaluation of the integral in (7) with the help of the experimental values of $d\Sigma/d\Omega$ yields Q values in the interval $(9\text{–}11)\cdot 10^{21}\,\text{cm}^{-4}$ for the various samples. Again, this result shows that the model being used here is valid within a few tenths.

2.2. Asymptotic behavior of the scattering cross section; fractal properties of the surface of the solid phase. Figure 3 shows asymptotic regions as $q \to \infty$ of the scattering curves, in logarithmic scale. The origin for the $\ln I$ scale has been shifted arbitrary distances for the various curves, in order to avoid intersections and superpositions of the curves. The

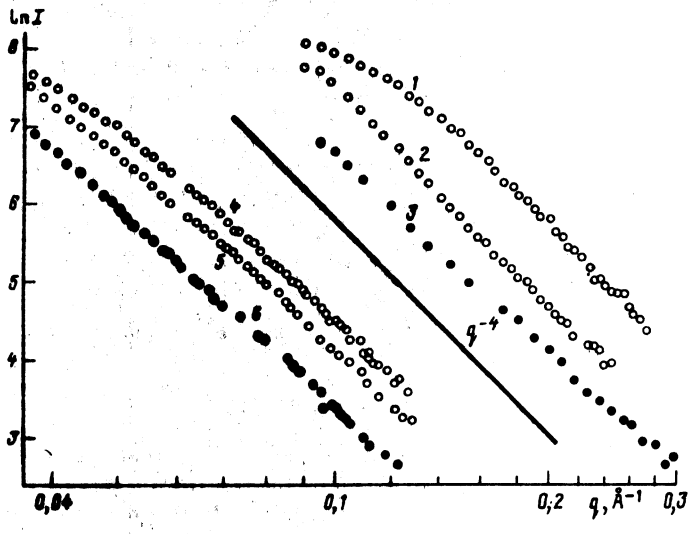

FIG. 3. I versus q, in full logarithmic scale, for several xerogel samples. 1—200 °C; 2—300 °C; 3—500 °C; 4—600 °C; 5—800 °C; 6—900 °C.

lines in this figure simply given an idea of the change in slope (or the change in n); they cannot be used for comparing intensities. We see that the $I(q)$ curves of all the test samples are described well in the limit $q \to \infty$ by the power law (1). Values of the Porod exponent n found from the slopes of the curves in Fig. 3 are shown in Table I. For the samples annealed at 900 °C, 800 °C, and 600 °C, the absolute intensity of the neutron scattering for q between 0.05 and 0.11 Å is high, and the low background does not affect the value of n. For the other samples, in contrast, the background must be considered more carefully. The scattering curves in the asymptotic region for the samples annealed at temperatures below 600 °C were analyzed with the help of the expression

$$I(q)=A+Bq^{-n}. \tag{8}$$

The exponent n for these curves was found by fitting (8) to the experimental results. Over the interval from 0.1 to 0.4 $Å^{-1}$, the background rises continuously with decreasing annealing temperature. The apparent reason for this result is the presence of a certain amount of crystallization water in the samples with the low annealing temperatures.

It follows from this table that the exponent n is approximately 4 for samples 1, 2, and 4. In order to find the scattering law (1) from expression (3), we must use an expression for $\gamma(r)$ as $r \to 0$ which is more accurate than that shown in Fig. 2. The exact value of $\gamma(r)$ as $r \to 0$ is known from Ref. 4 for the model under consideration here in the case of smooth inner surfaces:

$$\gamma(r)=1-\frac{r}{4c(1-c)}\frac{S_{tot}}{V}. \tag{9}$$

Here S_{tot} is the internal surface area, V is the volume, and $S=S_{tot}/V$ is the specific surface area per unit volume of the solid phase.

From (9) and (3) we find the following result in the limit $q \to \infty$:

$$\frac{d\Sigma}{d\Omega}=\frac{2\pi\rho^2 S}{q^4}. \tag{10}$$

We can use this expression to determine the specific area of the xerogel for smooth surfaces of the phase.

For the asymptotic law (1) with a noninteger n, the situation is more involved. In this case, for fractal interfaces, we have the following result from Ref. 12 for $r \to 0$:

$$\gamma(r)=1-\frac{N_0 r^{3-D_S}}{4c(1-c)}, \tag{11}$$

where N_0 is characteristic of a fractal boundary.

For objects with rough surfaces we have[13]

$$\gamma(r)=1-\frac{S_0 f b\,(r/a)^x}{4c(1-c)}, \tag{12}$$

where f is a numerical factor ~ 1, S_0 is the specific surface area if the roughness is ignored, b is a length, a is a lattice constant, and $x>0$.

The latter correlation functions lead to the expression[12,14]

$$\frac{d\Sigma}{d\Omega}=\frac{\pi(2-\Delta)(1-\Delta)\Gamma(1-\Delta)\sin[\pi(1+\Delta)/2]\rho^2}{q^4}S(q), \tag{13}$$

where Γ is the gamma function. We have

$$S(q)=N_0 q^{\Delta}\approx S_0(qR)^{\Delta}$$

for fractal boundaries (R is a characteristic dimension, and $\Delta=D_s-2$), and we have

$$S(q)=fS_0(b/a)\,(aq)^{\Delta} \quad (\Delta=1-x)$$

for rough boundaries.

A fundamental property of fractal entities is the dependence of their dimensions on the measurement scale. For example, the area of fractal surfaces measured with a scale r is

$$S_r=r^2\left(\frac{R}{r}\right)^{D_S}=R^2\left(\frac{R}{r}\right)^{\Delta}. \tag{14}$$

The same property is exhibited by rough surfaces with[13]

$$S_r\approx S_0\frac{w_r}{r}=S_0\frac{b}{a}\left(\frac{a}{r}\right)^{\Delta}. \tag{15}$$

Here we are assuming $w_r/r \gg 1$, where $w_r=b(r/a)^x$ determines the size of the fluctuations in the level of the rough surface with respect to the mean value, and $\Delta=1-x$. Expression (14) is the same as (15) if $b=a(R/a)^{\Delta}$ and $3-D_S=x$.

Comparing the expressions for $S(q)$ from (13) with (14) and (15), we conclude that neutron scattering measures the specific surface area at the scale q^{-1}. This conclusion explains the decrease in n from the value $n = 4$, corresponding to entities with a fractal surface.

The specific surface areas measured at a scale $q^{-1} = 10$ Å are listed in the last column in Table I. These areas were determined from (13) and the experimental values of the cross sections at $q = 0.1$ Å^{-1}. For the first three test samples, the specific surface areas were determined at $q = 0.182$ Å^{-1}, since the Porod region for these samples begins at $q > 0.1$, and the surface area does not depend on the measurement scale.

Since the areas found from (13) are areas per unit volume, Table I shows the values of this area divided by ρ_{sol}.

The decrease in $\Delta = D_S - 2$ to zero for samples 1, 2, and 4 may mean that the measurement scale q^{-1} for these samples is approaching the characteristic dimensions L_c and d_{coh}. Furthermore, we cannot rule out the possibility that the interfaces in these samples are being modified by hydroxyl groups, as was observed in Ref. 3. We also believe that the presence of definite length scales L_c and d_{coh} in the xerogel makes it possible to rule out the possibility that the results on small-angle neutron scattering in the Porod region might be explained by means of the distribution (2).

CONCLUSION

It can be concluded from these results that the Porod model, which we have used to describe the porous structure, successfully explains the experimental data on small-angle neutron scattering by samples of a xerogel of a solid solution of oxides of titanium, tin, and zirconium within a few tenths. In future work, it may be possible to achieve a further improvement in the accuracy with which the properties of the porous structure can be determined, through the use of a more realistic function $\gamma(r)$ and through precise measurements of the integral cross sections for scattering and absorption of our samples. These cross sections are required for calculating the scattering cross section $d\Sigma/d\Omega$.

One of us (É. Z. Valiev) wishes to thank S. V. Maleev for a discussion of these results.

[1] A. F. Wright, J. Non-Cryst. Solids **76**, 43 (1985).
[2] D. Schaefer and K. Kefer, in *Fractals in Physics* (Proceedings of the Sixth International Symposium on Fractals, Trieste, 1985) (Russ. Transl. Mir, Moscow, 1988, p. 62).
[3] M. J. Benham, J. C. Cook, *et al.*, Phys. Rev. B **39**, 633 (1989).
[4] A. Guinier and G. Fournet, *Small-Angle Scattering of X-Rays*, Wiley, New York, 1955, p. 78.
[5] G. Porod, Kolloid Z. **124**, 83 (1951); **125**, 51 (1952).
[6] L. M. Sharygin, V. F. Gonchar, and V. E. Moiseev, in *Ion Exchange and Ionometry*, Vol. 5, LGU, Leningrad, 1986, p. 9.
[7] J. D. F. Ramsay and R. O. Booth, J. Chem. Soc. **79**, 173 (1983).
[8] J. D. F. Ramsay, R. G. Avery, and L. Benest, Farad. Discuss. Chem. Soc. **76**, 53 (1983).
[9] P. Debye, H. R. Anderson, and H. Brumberger, J. Appl. Phys. **76**, 53 (1957).
[10] Ya. S. Umanskiĭ, *X-Ray Diffraction of Metals*, Moscow, 1967, pp. 45, 117.
[11] A. A. Feĭgin and D. I. Svergun, *Structure Analysis by Small-Angle X-Ray and Neutron Scattering*, Plenum, New York, 1987.
[12] H. D. Bale and P. W. Schmidt, Phys. Rev. Lett. **53**, 596 (1984).
[13] Po-zen Wong, Phys. Rev. B **32**, 7417 (1985).
[14] A. I. Okorokov, V. V. Runov, A. D. Tret'yakov, S. V. Maleev, and B. P. Toperverg, Preprint 1526, Leningrad Institute of Nuclear Physics, Leningrad, 1989.

Translated by D. Parsons